Mission Profile based Reliability Analysis of a Medium Voltage Power Conversion Architecture for PMSG based Wind Energy Conversion System

Sayan Acharya[a], Anup Anurag[a], Ghanshyamsinh Gohil[b], Samir Hazra[a], and Subhashish Bhattacharya[a]
[a]FREEDM Systems Center, North Carolina State University, Raleigh, NC 27606
[b]Department of Electrical Engineering, The University of Texas at Dallas, Dallas, TX 75080
Email: sachary@ncsu.edu, aanurag2@ncsu.edu, ghanshyam.gohil@utdallas.edu, shazra@ncsu.edu, and sbhatta4@ncsu.edu

***Abstract*—The development of wide-bandgap (WBG) power semiconductor devices has opened up new areas of applications which were previously dominated by silicon based IGBTs. This paper presents one such application where a multi-megawatt permanent magnet synchronous generator based wind energy conversion system (PMSG-WECS) is used for medium voltage (MV) grid integration. The conversion of the low output voltage of the PMSG to medium voltage brings about a multitude of advantages including reduction in the cable diameter and consequently the cost and weight of the system. WBG devices enable the use of high frequency transformers which makes it possible to install the system on the tower of the wind turbine. With these kinds of installations, it becomes necessary to investigate the reliability of the system, since maintenance of the systems leads to additional incurred costs. This paper provides a mission-profile (i.e. wind speed and ambient temperature) based analysis, in order to determine the temperature rise in the devices and consequently, its effects on the lifetime of the devices. An analytical lifetime model has been used and the damage produced on the transistors has been quantified using Palgrem Miner rule. This analysis can be helpful in understanding the impacts of having a tower-top converter system on the overall cost.**

***Index Terms*—Foster Thermal model, Modular Converter, Permanent Magnet Synchronous Motor, Reliability, Silicon Carbide devices, Thermal Performance, Wind Energy Conversion Systems (WECS)**

I. Introduction

THE past few years have experienced a widespread growth in wind power generating capacity. According to the world wind energy market, the year 2017 witnessed 52 GW of new installations [1]. Fig. 1 shows the global cumulative installed wind capacity for the last seventeen years.

Increased penetration and stochastic nature of the wind demands more controllability of Wind Turbine (WT) and requires WT to provide ancillary services for wide spread adoption and smooth grid integration. The doubly-fed induction generator (DFIG) with partial-scale power converter (WT type C) and permanent magnet synchronous generator (PMSG) with full-scale power converter (WT type D) are generally used. The DFIG provided advantages in terms of its weight, lower maintenance costs and lower cost per KW since the converter for these system are 30% of the rated power [2], [3]. Compared to the DFIG based concept, the PMSG provides advantages

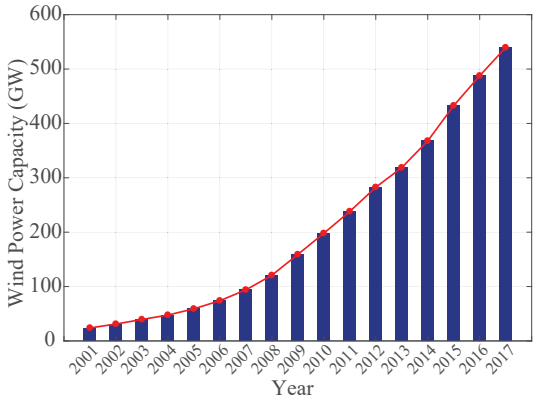

Fig. 1: Global Cumulative Installed Wind Capacity. An increasing trend is noticed in the wind power installed capacity owing to the maturity of the technology while competing successfully with heavily subsidized incumbent technologies [1].

due to the elimination of the slip rings, full power and speed controllability and simpler or even no gearbox structures. But since now the converter has to be rated for full power the total system efficiency would reduce for WT type D systems. However, in the event of the grid faults, type D wind turbine demonstrates better controllability compared to the type C and therefore it is most preferred solution for new installations in the countries with the stringent grid codes.

MV PMSGs (in ranges of 4.16 kV) are bigger in size as compared to their LV (690 V) counterparts due to the insulation requirements. Therefore, LV PMSGs are generally preferred for lower power levels. With the increase in power levels, the LV PMSGs (with LV converters) suffer from a major disadvantage due to the fact that the current rating of the cables becomes high. This increases the weight and the cost of the entire system. A line-frequency transformer can be a solution for stepping up the voltage rating in order to reduce the current ratings. However, the line-frequency transformer is bulky and expensive [5]. This calls for an approach to replace the line frequency transformers by solid state transformers (SSTs) in order to enable MV integration with the grid [6]. With the multitude of advantages offered by the SST, the use of power semiconductor devices brings forward reliability issues

978-1-5386-4536-9/18/$31.00 © 2018 IEEE

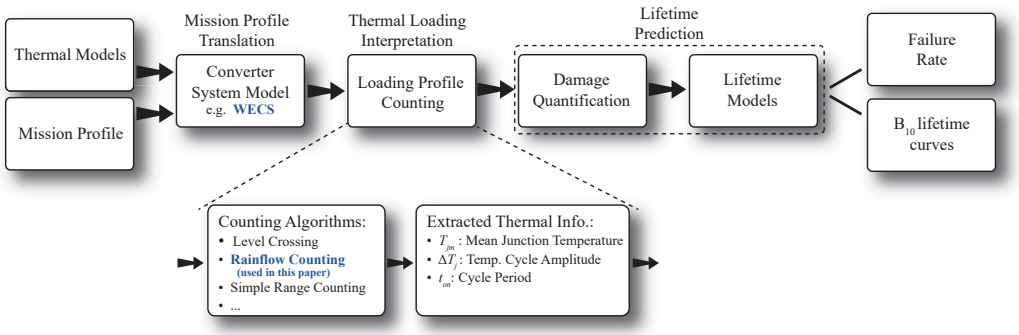

Fig. 2: Flowchart for the reliability analysis of power devices caused by long term thermal cycles [4].

which are not very prominent in line-frequency transformers. In addition, the reduction in the converter size enables tower top installation of the converters which makes their reliability analysis even more important.

The main components of the power converter used for such a system include power switching devices (MOSFETs or IGBTs and diodes), dc-link capacitors and high frequency transformers (HFTs) [7], [8]. Numerous factors like thermal stress, mechanical stress etc. can cause failure in the power devices. However, the most frequently observed failure mechanism is attributed to the thermal stresses caused by the temperature swings and the increased mean junction temperature in the device [9], [10].

In this paper, a thermal and reliability analysis has been carried out on the power semiconductor devices using the procedure shown in Fig. 2. Rainflow analysis method is used to identify the corresponding temperature swings of each thermal cycle. An analytical lifetime model is used and the damage is quantified by Palgrem Miner rule. The reliability of the dc-link capacitors and the high-frequency transformers have not been taken into account in this study.

II. 13.8 kV, 5 MW Wind Energy Converter

The wind energy converter as depicted in [5] is taken for analysis. It should be noted that the cascaded H-bridge structure as shown in Fig. 3(a) is built using SiC MOSFETs. Although these devices have a comparatively lower current rating than silicon IGBTs (with similar voltage ratings), the operating frequency can be pushed to much higher values which helps in reducing the size of the magnetics [11].

A. Topology of the Wind Energy Converter

The grid side AFEC is based on a two-stage modular structured power converter. Each module has a ac-dc stage followed by an high frequency isolated dc-dc stage. The input ac-dc stage is star connected CHB structure where ten H-bridges are connected in series in each phase and the output of the isolated dc-dc stages are connected in parallel. The dc-dc converter is based on single phase Dual Active Bridge (DAB) which provides the galvanic isolation through the high frequency transformer [12], [13].

With this configuration, a maximum of twenty-one level phase voltage can be generated. This helps in reducing the harmonic contents in the voltage which in turn reduces passive filtering requirements on the grid side. The system parameters are listed in Table I. The PMSG side converter system is not considered for this analysis.

TABLE I: Parameters of the system

Dual Active Bridge (DAB)		*13.8 kV input side CHB*	
No. of DABs	30	No. of H-bridges	30 (10 H-bridges per phase)
Devices used	CAS300M17BM2	Device used	CAS300M12BM2
Turns ratio of HFT	1:1	Grid side Inductance	2.5
VA rating of HFT	167 kVA		
Operating frequency of HFT	10 kHz	Switching Frequency	5 kHz
System Inertia Constant		75 ms	

B. Control Strategy implemented for the CHB of the wind energy converter

This stage interfaces the system to the MV grid (13.8 KV). Each of the H-bridge DC bus is actively controlled at 1.2 kV. This paper adopts a phase-shifted-PWM technique to control the individual dc buses [14], [15]. With this technique an effective switching frequency of 90 kHz is achieved which reduces the filter requirements for the grid side. The average dc bus controller generates the d-axis current reference and the q-axis current reference is set as zero as unity power factor operation is desired. The average dc bus PI controller is designed based on the power balance model [16]. The bandwidth of the average dc bus PI controller is kept at one tenth of the dq-axis current controller bandwidth to maintain the system stability. Fig. 3(b) shows the implemented system level controller.

III. Performance Evaluation of the 1.7 kV SiC MOSFET based Power Block

The key element in building the whole converter system is the 1.7 kV SiC-MOSFET module [17]. Wolfspeed CAS300M17BM2 module is used as the semiconductor switch on the MV side converter in this design [18].

A. Electrical Performance

The module performance is evaluated by performing Double Pulse Tests (DPT) since the exact conditions for the swithing energy results are not provided on the datasheet. The total switching loss as a function of device current is presented in Fig. 4(a). As compared to the same rated Si-IGBTs the total

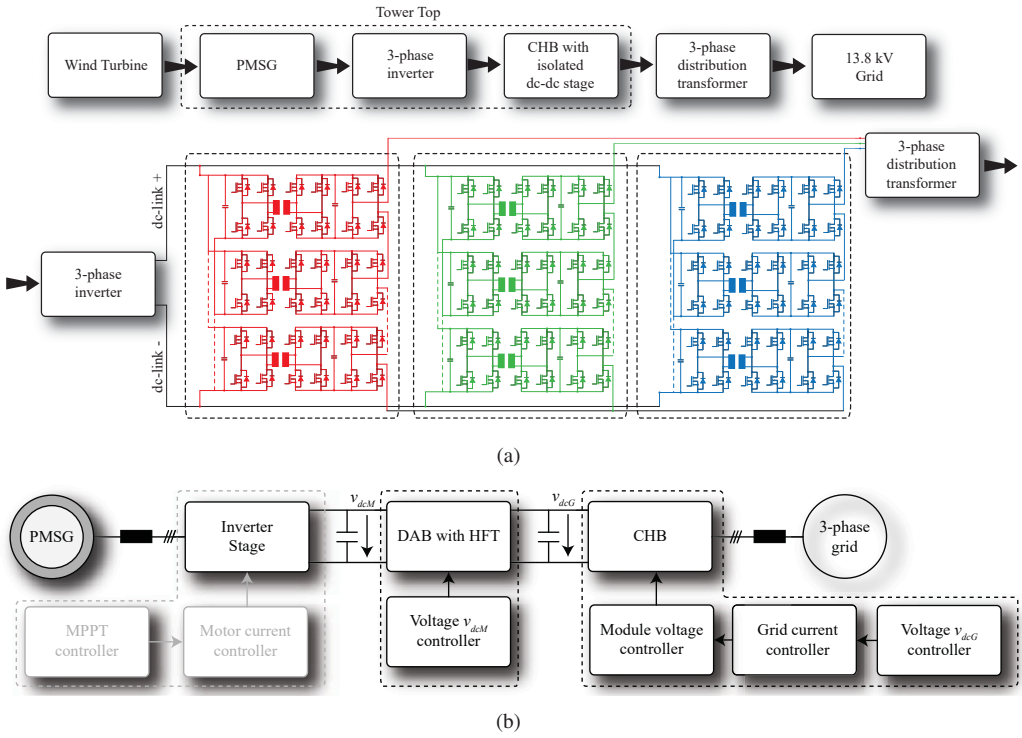

Fig. 3: (a) Schematic of the PMSG based solution with a cascaded H-bridge structure built with SiC MOSFETs. The power conversion stage is designed in a modular fashion and has two stages: MV output stage at the 13.8 kV grid side and the LV input side at the PMSG. (b) Control structure of the WECS. The control for the PMSG is not carried out in this study and the torque reference for the generator is provided manually.

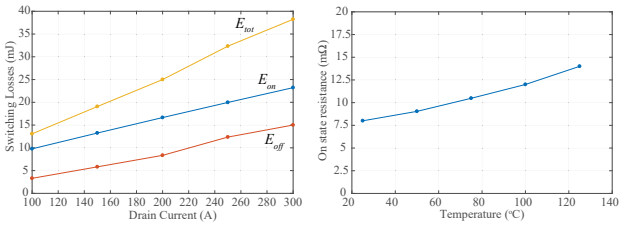

Fig. 4: (a) Switching Losses for the SiC MOSFET module CAS300M17B2. The switching losses are measured at room temperature. The relation between the switching energy and temperature is extracted from the datasheet and an extrapolation technique is used for calculating the switching energy losses at higher temperatures. (b) On-state resistance of SiC MOSFET module CAS300M17B2. The values are directly taken using an LCR meter. Measurements with the LCR meter provides identical results as provided in the datasheet.

switching loss is much less for this SiC-MOSFET. The on-state resistance values are measured using a LCR meter [19] and is shown in Fig. 4(b) and is the values are compared to the datasheet.

B. Thermal Performance

The electrical performance of a device is directly linked with its thermal behavior through the power losses on the device [20]. The conduction losses and the switching losses which mainly constitutes the power losses are the main source of temperature rise. An accurate thermal model is therefore, imperative to estimate the junction temperature. The thermal model of the MOSFET module is provided in Fig. 5. It is based on the Foster model [21]. A Foster model is used since the parameters can be easily found from the datasheet. The power loss in the MOSFET is dissipated through its junction to case thermal resistance ($R_{th(j-c)}$) which causes the junction temperature of the MOSFET (T_{jM}) to rise above the ambient temperature (T_{amb}).

The power losses in the diode are also evaluated and a similar analysis is made based on the Foster model. However, it should be noted that in case of SiC MOSFETs, the channel conducts in the reverse direction (third quadrant operation) making the diode conduct only during the deadtime [22]. This leads to very low power losses in the diode as compared to the MOSFET and hence the damage quantification due to the diode temperature rise is not taken into account. The cross effect of the MOSFET temperature rise with the diode temperature rise is beyond the scope of the paper.

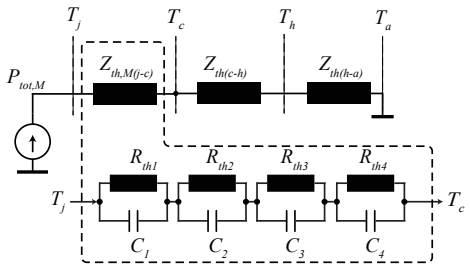

Fig. 5: Thermal model of a single device in the MOSFET module. The thermal model of the diode is not provided here since the total losses in the diode is very low and it is not included in the analysis [9].

IV. Mission Profile Based Analysis

Conventional analysis procedures are generally focused on calculating the power losses under certain constant conditions. This, however, might provide unreliable results since it does not reflect the real field environment. With the introduction of real time monitoring systems, accurate mission profile data (i.e. wind speed and ambient temperature) are available [23]. In order to analyze the reliability of a system it is imperative to take the mission profile into consideration [24], [25]. The mission profile can be a series of multi-time scales, for example, a minute mission profile or a yearly mission profile, and it is usually taken as the input for the loss analysis in the field of power electronics converters [9]. The mission profiles are different in different places and in different seasons. Therefore, it becomes necessary to investigate the reliability of power converter systems not only in short-term conditions but also long term durations. Table II highlights the major system parameters used for the analysis. The simulation is carried out in PLECS [26].

TABLE II: Parameters used in the simulation

Dual Active Bridge (DAB)		*13.8 kV input side CHB*	
Input dc-link voltage	1.2 kV	Input dc-link voltage	1.2 kV
Output dc-link voltage	1.2 kV	Output ac rms voltage	800 V
Operating frequency of HFT	10 kHz	Switching Frequency	5 kHz
Power rating		166.6 kW	
Device used		CAS300M17BM2	
Gate Resistance		5 Ω	
DC-link capacitor		4.7 mF	

A. Power generated by the wind turbine

The electrical power generated by the wind turbine is obtained using a power curve.

$$P(v) = \begin{cases} 0, & v < v_{ci} \text{or } v > v_{co} \\ q(v) & v_{ci} \le v \le v_r \\ P_r, & v_r \le v \le v_{co} \end{cases}$$

where v_{ci}, V_{co} and v_r is the cut-in speed, cut-out speed and the rated speed, respectively. P_r denotes the rated power of the wind turbine. The exponential power curve is given by

$$q(v) = \frac{1}{2}\rho A k_p (v^{\epsilon} - v_{ci}^{\epsilon}) \quad (1)$$

where ρ is the air density (generally 1.225 kg/m^3) and A is the rotor area. k_p and ϵ are constants. Fig. 6 shows the power profile of the wind turbine taken for analysis in this paper.

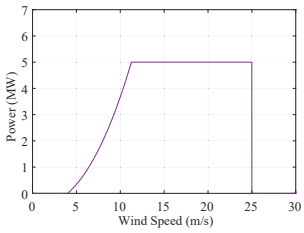

Fig. 6: Power curve for the 5 MW, 690 V wind turbine with area A = 18627 m^2, k_p = 1.8382, ϵ = 2.3

B. Estimation of operational losses and junction temperature rise in the SiC MOSFET

The mission profile based analysis starts with the estimation/measurement of the various losses and consequently the increase in junction temperature, that occurs in the device at all the operating points. Fig. 7(a) shows the total losses occurring in one device along its whole operating range.

In order to calculate the junction temperature rise, the thermal parameters of the device are fed into the simulation. The parameters of the heatsink are based on realistic values. In Fig. 7(b), the variation of the maximum junction temperature over the whole operating range is depicted.

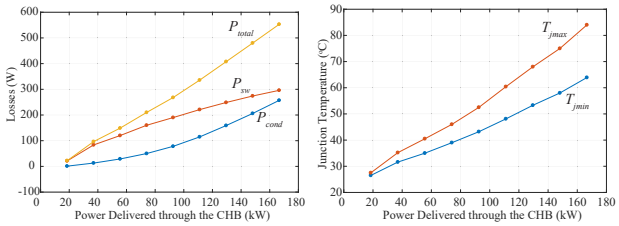

(a) (b)

Fig. 7: (a) Conduction losses, switching losses and total losses seen by one device of the CHB through its full operating range. The gate resistance is kept at 5 Ω for the whole operation. (b) Maximum and minimum junction temperature of the MOSFET. The ambient temperature is taken to be 25^{o}C.

C. Thermal Loading Profile

The thermal loading profile of the PMSG based WECS under a yearly mission profile (Fig. 8) is shown in Fig. 9. The calculation is based on a lookup table based method where the losses and maximum junction temperature and calculated for specific values of power injection. The mission profile is then served as an input for this lookup table. It should be noted that the variation in the power output due to change in temperature (on account of changing air density) is not taken into account. The increased junction temperature and the junction temperature swings are the main precursor for the failure of the device.

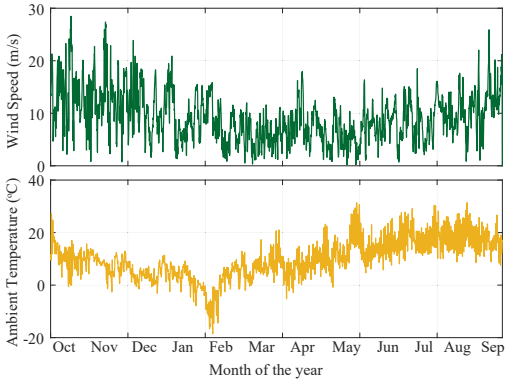

Fig. 8: Yearly mission profiles from recorded data (3 h per sampling data). The mission profile shows the wind speed at the ambient temperature for a particular area. This profile changes depending on the site of installation. The analysis shown in the paper is for this particular profile and the lifetime of the converter might change depending on the wind profile and ambient temperature at the location.

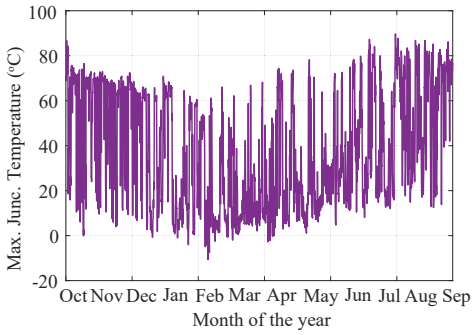

Fig. 9: Maximum junction Temperature of the MOSFET considering the mission profile shown in Fig. 8. The junction temperature raises above the ambient depending on the power profile which is the main precursor for device failure.

V. Lifetime Estimation

The lifetime estimation for the long term mission profile is carried out and statistical techniques have been used to estimate the damage and lifetime of one device. It should be noted that the estimated lifetime is only for one device and does not include the lifetime of the capacitors or other components of the WECS.

A. Rainflow Method

A rainflow counting method [27], [28] is employed on the long term thermal loading profile. This helps in the conversion of randomly changing thermal loading profiles to regulated thermal cycles. The rainflow counting method which extracts the change in junction temperature (ΔT_j), mean junction temperature (T_{jm}) and the number of cycles (t_{cycle}) is used in this paper. The counting results for thermal loading is shown in Fig. 10 where a total of 563 thermal cycles have been identified.

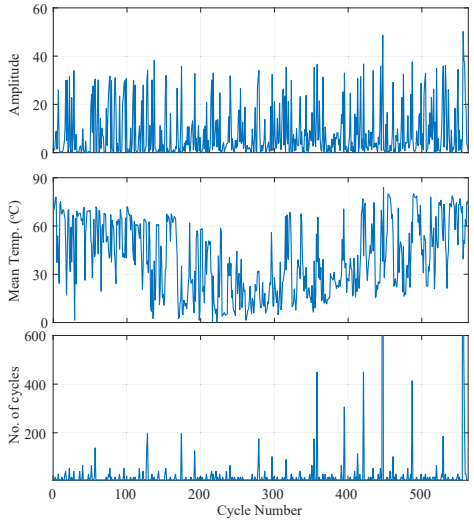

Fig. 10: Rainflow counting results of the junction temperature profile with the given temperature profile.

B. Lifetime Model and Damage Analysis

A lifetime model is used to estimate the total remaining life of the device. Different methods have been provided in the literature [29]. A lifetime model for Si IGBT (SKiM 63) [9] has been used in this analysis since the research on the lifetime models for SiC MOSFETs is currently ongoing [30]. However, the state-of-the-art Si lifetime model provides a good estimation for the lifetime since it is based on the packaging of the device.

$$N_f = A \times (\Delta T_j)^{\alpha} \times (ar)^{\beta_1 \Delta T_j + \beta_0} \times \left[\frac{C + (t_{ON})^{\gamma}}{C+1}\right] \times \exp\left(\frac{E_a}{k_b \times T_{\text{jm}}}\right) \times f_{\text{diode}} \quad (2)$$

where A, α, β_0, β_1, γ and C are the model parameters as shown in [30]. ar is the bond wire aspect ratio, f_{diode} is the diode chip-thickness and t_{ON} is the cycling period.

The damage modeling is done using Palgrem-Miner's rule [31] which states that the accumulated life consumption is linearly dependent on the contribution of different thermal cycles.

$$LC = \sum_i \frac{n_i}{N_{fi}} \quad (3)$$

number of cycles to fail. Here, the particular value of LC for each cycle or each half-cycle is given by [31]

$$LC_i = \frac{n_i}{N_{fi}} \quad (4)$$

where i is the cycle number.

The expected lifetime can be calculated from the damage caused by the identified cycles in t_{MP} which is the mission profile period, as

$$LF = \frac{t_{\text{MP}}}{LC} \quad (5)$$

The accumulated damage is calculated for the long term

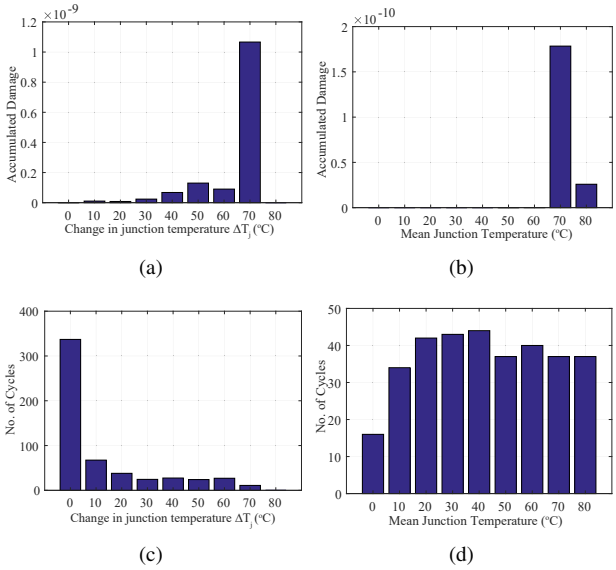

Fig. 11: Rainflow Analysis results (a) Accumulated damage vs change in junction temperature (b) Accumulated damage vs mean junction temperature (c) No. of cycles vs change in junction temperature (d) No. of cycles vs mean junction temperature.

mission profile and it comes out to be $LC = 1.5701 \times 10^{-9}$. The expected lifetime from (5) comes out to be 20.2 years.

This provides an idea regarding the lifetime of the CHB in a WEC system. This analysis is based on the assumption that there is no other incident on the device which might cause it to degrade or fail.

VI. Conclusion

This paper analysis the reliability of a CHB in a MV power conversion topology which interfaces a 690 V, MW PMSG with a 13.8 kV grid directly based on a mission profile approach. The use of SiC MOSFETs enables the converter to use high frequency transformers allowing tower top placement of the power electronics system. Even though the tower top placement of the power electronics converter system reduces the ground footprint, the cost of the maintenance of the system increases. This calls for a reliability based analysis of the power electronic converter. This analysis is helpful in determining the relation between total cost and size of the system and the cost incurred for maintenance. A mission-profile based analysis is carried out taking into account the wind profile and ambient temperature at a particular place and estimating the damage and consequently the lifetime of the system. In future, this analysis can be extended to determine the lifetime of capacitors and the silicon based IGBT converter, which can ensure the maintenance intervals more accurately.

References

[1] "Global Wind Statistics 2017," http://gwec.net/global-figures/graphs/, accessed: 2018-03-12.

[2] F. Blaabjerg and K. Ma, "Future on Power Electronics for Wind Turbine Systems," *IEEE Journal of Emerging and Selected Topics in Power Electronics*, vol. 1, no. 3, pp. 139–152, Sept 2013.

[3] G. Gohil, R. Teodorescu, T. Kerekes, F. Blaabjerg, and S. Battacharya, "Mission-profile based multi-objective optimization of power electronics converter for wind turbines," in *2017 IEEE Energy Conversion Congress and Exposition (ECCE)*, Oct 2017, pp. 3514–3521.

[4] A. Anurag, Y. Yang, and F. Blaabjerg, "Reliability analysis of single-phase PV inverters with reactive power injection at night considering mission profiles," in *2015 IEEE Energy Conversion Congress and Exposition (ECCE)*, Sept 2015, pp. 2132–2139.

[5] S. Acharya, S. Hazra, K. Vechalapu, and S. Bhattacharya, "Medium voltage power conversion architecture for high power PMSG based wind energy conversion system (WECS)," in *2017 IEEE Energy Conversion Congress and Exposition (ECCE)*, Oct 2017, pp. 3329–3336.

[6] J. E. Huber and J. W. Kolar, "Solid-State Transformers: On the Origins and Evolution of Key Concepts," *IEEE Industrial Electronics Magazine*, vol. 10, no. 3, pp. 19–28, Sept 2016.

[7] S. Bal, A. K. Rathore, and D. Srinivasan, "Naturally Clamped Snubberless Soft-Switching Bidirectional Current-Fed Three-Phase Push-Pull DC/DC Converter for DC Microgrid Application," *IEEE Transactions on Industry Applications*, vol. 52, no. 2, pp. 1577–1587, March 2016.

[8] A. Anurag and B. C. Babu, "Control of Grid Connected Inverter system for Sinusoidal Current Injection with Improved Performance," in *2012 Students Conference on Engineering and Systems*, March 2012, pp. 1–6.

[9] A. Anurag, Y. Yang, and F. Blaabjerg, "Thermal Performance and Reliability Analysis of Single-Phase PV Inverters With Reactive Power Injection Outside Feed-In Operating Hours," *IEEE Journal of Emerging and Selected Topics in Power Electronics*, vol. 3, no. 4, pp. 870–880, Dec 2015.

[10] G. Mandrusiak, X. She, A. M. Waddell, and S. Acharya, "On the Transient Thermal Characteristics of Silicon Carbide Power Electronics Modules," *IEEE Transactions on Power Electronics*, vol. PP, no. 99, pp. 1–1, 2018.

[11] A. Hussein, A. Castellazzi, P. Wheeler, and C. Klumpner, "Performance benchmark of Si IGBTs vs. SiC MOSFETs in small-scale wind energy conversion systems," in *2016 IEEE International Power Electronics and Motion Control Conference (PEMC)*, Sept 2016, pp. 963–968.

[12] J. Everts, F. Krismer, J. V. den Keybus, J. Driesen, and J. W. Kolar, "Optimal ZVS Modulation of Single-Phase Single-Stage Bidirectional DAB AC/DC Converters," *IEEE Transactions on Power Electronics*, vol. 29, no. 8, pp. 3954–3970, Aug 2014.

[13] V. M. Iyer, S. Gulur, and S. Bhattacharya, "Optimal design methodology for dual active bridge converter under wide voltage variation," in *2017 IEEE Transportation Electrification Conference and Expo (ITEC)*, June 2017, pp. 413–420.

[14] L. Maharjan, S. Inoue, H. Akagi, and J. Asakura, "State-of-Charge (SOC)-Balancing Control of a Battery Energy Storage System Based on a Cascade PWM Converter," *IEEE Transactions on Power Electronics*, vol. 24, no. 6, pp. 1628–1636, June 2009.

[15] S. Acharya, K. Vechalapu, S. Bhattacharya, and N. Yousefpoor, "Comparison of DC fault current limiting capability of various modular structured multilevel converters within a multi-terminal DC grid," in *2015 IEEE Energy Conversion Congress and Exposition (ECCE)*, Sept 2015, pp. 3184–3191.

[16] M. Hagiwara and H. Akagi, "Control and Experiment of Pulsewidth-Modulated Modular Multilevel Converters," *IEEE Transactions on Power Electronics*, vol. 24, no. 7, pp. 1737–1746, July 2009.

[17] S. Hazra, A. De, L. Cheng, J. Palmour, M. Schupbach, B. A. Hull, S. Allen, and S. Bhattacharya, "High Switching Performance of 1700-V, 50-A SiC Power MOSFET Over Si IGBT/BiMOSFET for Advanced Power Conversion Applications," *IEEE Transactions on Power Electronics*, vol. 31, no. 7, pp. 4742–4754, July 2016.

[18] "CAS300M17BM2: 1700-V, 8.0-mΩ, Silicon Carbide, Half-Bridge Module," https://www.wolfspeed.com/cas300m17bm2, accessed: 2018-03-12.

[19] "E4980AL Precision LCR Meter 20 Hz to 300 kHz/500 kHz/1 MHz ," https://www.keysight.com, accessed: 2018-03-12.

[20] E. Romero-Cadaval, G. Spagnuolo, L. G. Franquelo, C. A. Ramos-Paja, T. Suntio, and W. M. Xiao, "Grid-Connected Photovoltaic Generation Plants: Components and Operation," *IEEE Industrial Electronics Magazine*, vol. 7, no. 3, pp. 6–20, Sept 2013.

[21] Y. Yang, H. Wang, F. Blaabjerg, and K. Ma, "Mission profile based multi-disciplinary analysis of power modules in single-phase transformerless photovoltaic inverters," in *2013 15th European Conference on Power Electronics and Applications (EPE)*, Sept 2013, pp. 1–10.

[22] G. Tolstoy, P. Ranstad, J. Colmenares, D. Peftitsis, F. Giezendanner, J. Rabkowski, and H. P. Nee, "An experimental analysis on how the dead-time of SiC BJT and SiC MOSFET impacts the losses in a high-frequency resonant converter," in *2014 16th European Conference on Power Electronics and Applications*, Aug 2014, pp. 1–10.

[23] H. Wang, K. Ma, and F. Blaabjerg, "Design for reliability of power electronic systems," in *IECON 2012 - 38th Annual Conference on IEEE Industrial Electronics Society*, Oct 2012, pp. 33–44.

[24] Y. Yang, A. Sangwongwanich, and F. Blaabjerg, "Design for reliability of power electronics for grid-connected photovoltaic systems," *CPSS Transactions on Power Electronics and Applications*, vol. 1, no. 1, pp. 92–103, Dec 2016.

[25] K. Ma, H. Wang, and F. Blaabjerg, "New Approaches to Reliability Assessment: Using physics-of-failure for prediction and design in power electronics systems," *IEEE Power Electronics Magazine*, vol. 3, no. 4, pp. 28–41, Dec 2016.

[26] "Plexim: Electrical Engineering Software," https://www.plexim.com, accessed: 2018-03-12.

[27] "Standard practices for cycle counting in fatigue analysis," *ASTM International, IEEE Standard E1049-85*, 2005.

[28] K. Ma, M. Liserre, F. Blaabjerg, and T. Kerekes, "Thermal Loading and Lifetime Estimation for Power Device Considering Mission Profiles in Wind Power Converter," *Power Electronics, IEEE Transactions on*, vol. 30, no. 2, pp. 590–602, Feb 2015.

[29] C. Busca, R. Teodorescu, F. Blaabjerg, S. Munk-Nielsen, L. Helle, T. Abeyasekera, and P. Rodriguez, "An overview of the reliability prediction related aspects of high power IGBTs in wind power applications," *Microelectronics Reliability*, vol. 51, no. 9, pp. 1903 – 1907, 2011, proceedings of the 22th European Symposium on the Reliability of Electron Devices, Failure Physics and Analysis.

[30] N. C. Sintamarean, F. Blaabjerg, H. Wang, and Y. Yang, "Real Field Mission Profile Oriented Design of a SiC-Based PV-Inverter Application," *IEEE Transactions on Industry Applications*, vol. 50, no. 6, pp. 4082–4089, Nov 2014.

[31] A. Niesony, "Determination of fragments of multiaxial service loading strongly influencing the fatigue of machine components," *Mechanical Systems and Signal Processing*, vol. 23, no. 8, pp. 2712 – 2721, 2009.